Trade-off between safety, mobility and stability in automated vehicle following control: Theories and field experiments

Xiaopeng Li, Associate Professor
University of South Florida

2021/4/16
Webinar Series
TRB Committee on Traffic Flow Theory and Characteristics

High Hopes on Automated Vehicles (AVs)

- Safety: >94% reduction of crashes (Winkle, 2016)
- Mobility: capacity tripled (Varaiya, 1993; Ioannou 1997) ; quadrupled (Karaaslan, 1990)
- Energy efficiency: +25-50% (Vahidi & Sciarretta, 2018)

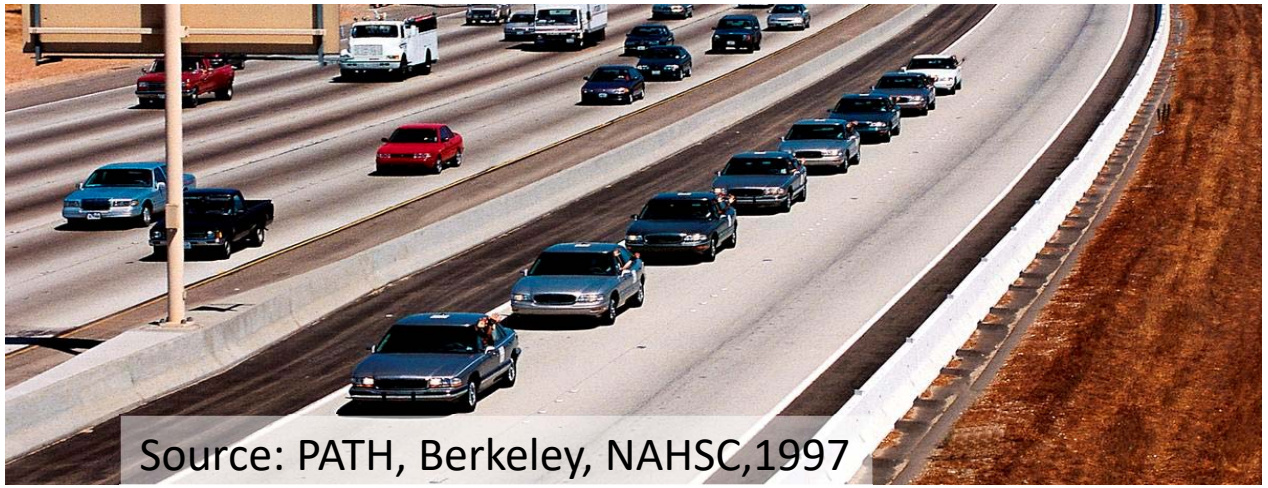

Source: PATH, Berkeley, NAHSC,1997

Current Status – Technology Deployment

- Production AVs market penetration rates
  - 2% in 2015 -> 10% in 2025 -> 40% in 2040.

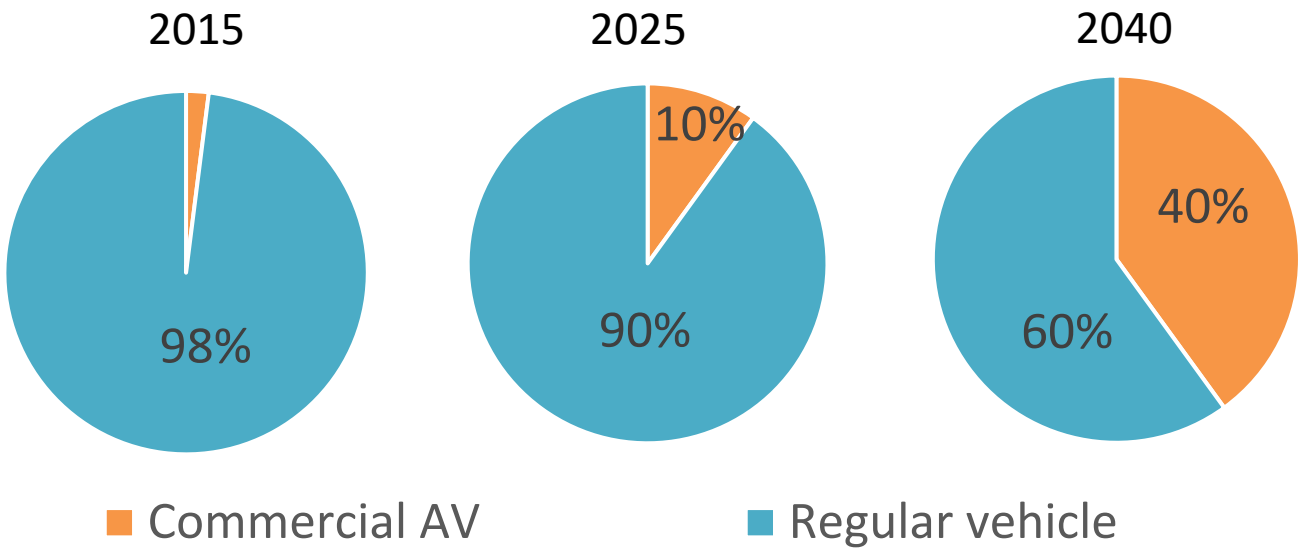

Current Status – Technology Deployment

- Production AVs market penetration rates
  - 2% in 2015 -> 10% in 2025 -> 40% in 2040.
- Advanced Driver-Assistance Systems (ADAS)
  - Longitudinal – adaptive cruise control (ACC)

Adaptive Cruise Control (ACC)

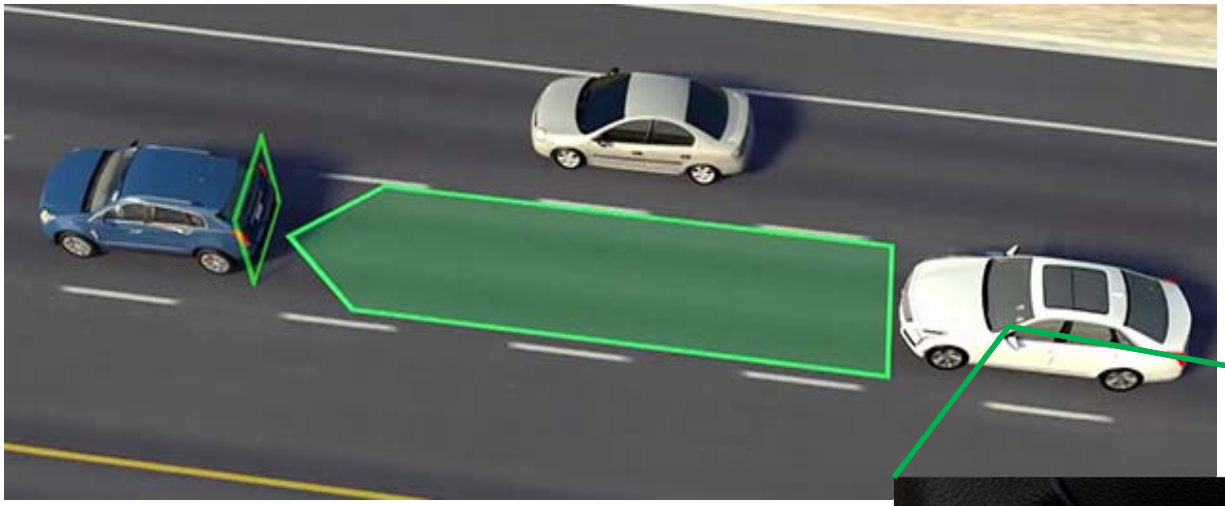

Following speed setting

Following headway setting

Source: https://owner.ford.com/support/how-tos/safety/driver-assist-technology/cruise-control/how-to-use-adaptive-cruise-control.html#
https://my.cadillac.com/how-to-support/driving-performance/driving/adaptive-cruise-control

Existing Studies

- **Microscopic impacts of AVs**

Microscopic level models (e.g., car-following models, lane-changing models) directly describe interactions between individual vehicles and resulting dynamics.

There are abundant AV following models studies, e.g., Lenard, 1970; Ghiasi et al., 2017; Jerath and Brennan, 2012; Kesting et al., 2010; Khosravi et al., 2018; Ngoduy, 2013; Seiler et al., 2004; Treiber and Kesting, 2013.

- **Gaps**

- Most of them were simulation-based studies, some findings were inconsistent with those from field experiments.
- Among those field-experiment-based studies, rationale of the string-unstable design of commercial AV control still is unclear. Also, the adopted AV following models are simple linear models.
- Commercial AVs often offer users to customize the AV following headway among different levels, which may have significant impacts on traffic mobility, stability, and energy consumption.

Implications to Macroscopic Traffic

- **Macroscopic impacts of AVs**

Macroscopic level models (e.g., fundamental diagram (FD)) study the relationships among traffic flow characteristics, e.g., density, flow rate, speed of a traffic stream.

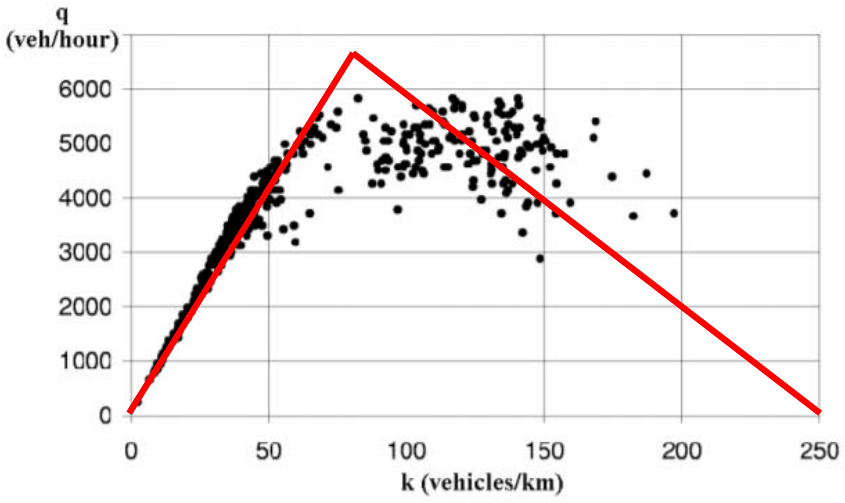

Existing studies on macroscopic AV traffic characteristics focused on the impacts of AVs on the traffic flow capacity, e.g., Arnaout and Arnaout, 2014; Ghiasi et al., 2019, 2017; Liu et al., 2018; Shladover et al., 2012; Van Arem et al., 2006.

- **Gaps**

➢ FD investigation for pure AV or mixed HV and AV traffic is scarce.

➢ Existing studies modeled FD with simple analysis or pure simulation with very optimistic assumptions of AV controls.

Outline

Field Experiments

Theoretical Analysis

Implication to Macroscopic Traffic

AV Trajectory Data Collection

❖ Facilities

- Lincoln MKZ 2016 (red)
- Lincoln MKZ 2017 (black)
- Four headway settings (1 to 4 from short to long)

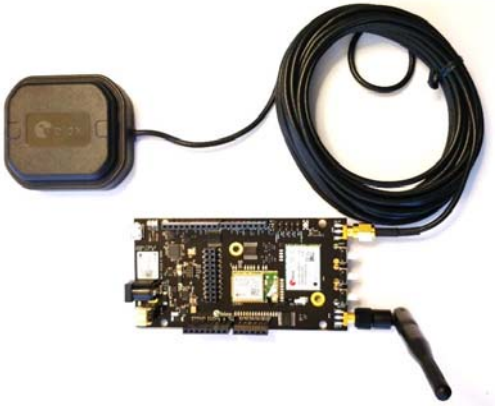

- U-blox GNSS receiver
- Position accuracy: ±0.26 m
- Speed accuracy: ±0.089m/s

AV Trajectory Data Collection

❖ **Testing sites**

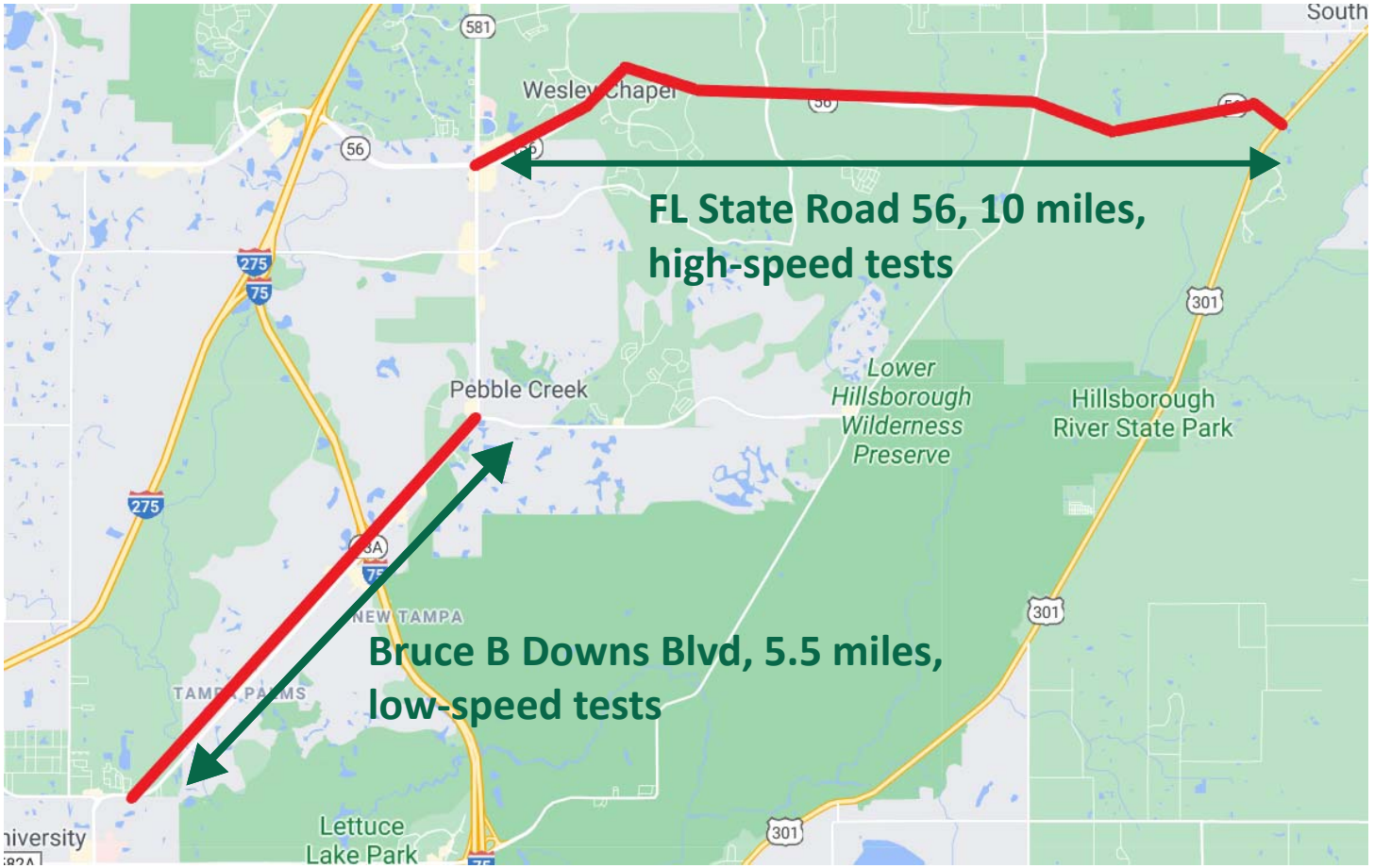

AV Trajectory Data Collection

❖ Experiment settings

- Car-following experiment

- Platooning experiment


: regular vehicle with a cruise control system

AV Trajectory Data Collection

❖ **Experiment settings**

Test number	v_I (mph)	v_T (mph)	Test number	v_I (mph)	v_T (mph)
1	55	53	**11**	35	33
2	55	53	**12**	35	33
3	55	51	**13**	35	31
4	55	51	**14**	35	31
5	55	49	**15**	35	29
6	55	49	**16**	35	29
7	55	47	**17**	35	27
8	55	47	**18**	35	27
9	55	45	**19**	35	25
10	55	45	**20**	35	25

v_I: the initial speed of the lead vehicle; v_T: the target speed of the lead vehicle.

AV Trajectory Data Collection

❖ Car-following data illustration

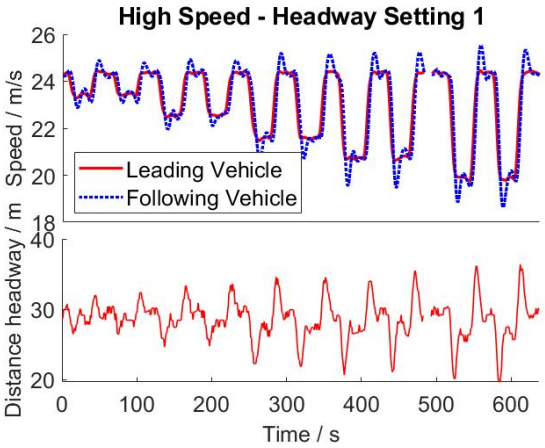

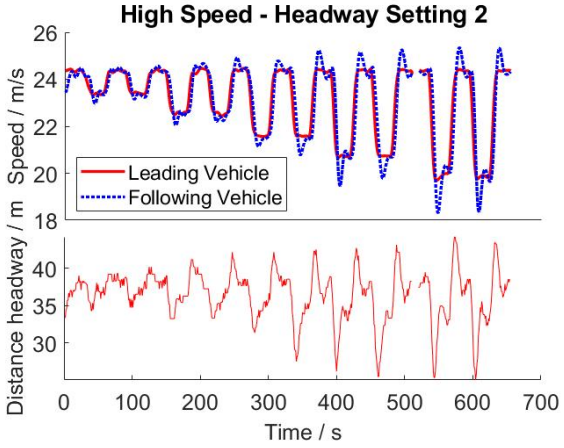

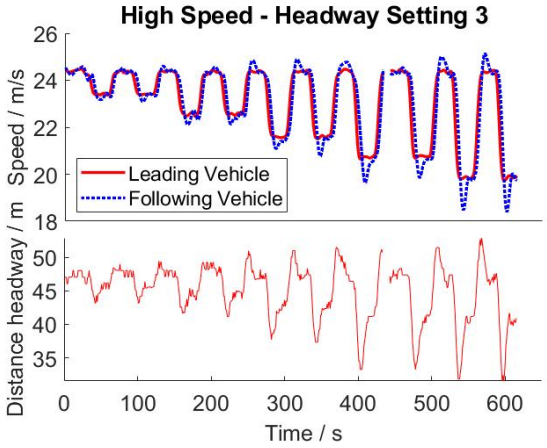

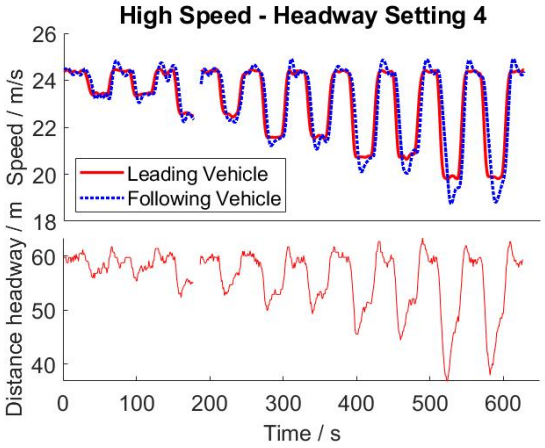

AV Trajectory Data Collection

❖ Platooning data illustration

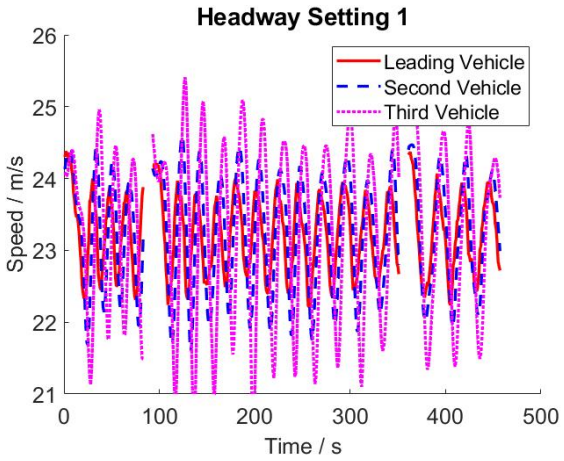

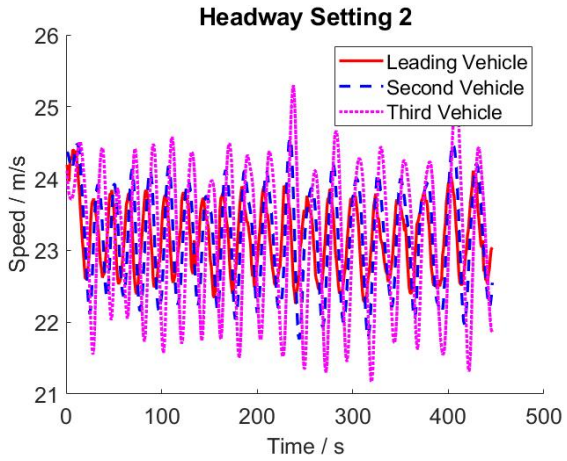

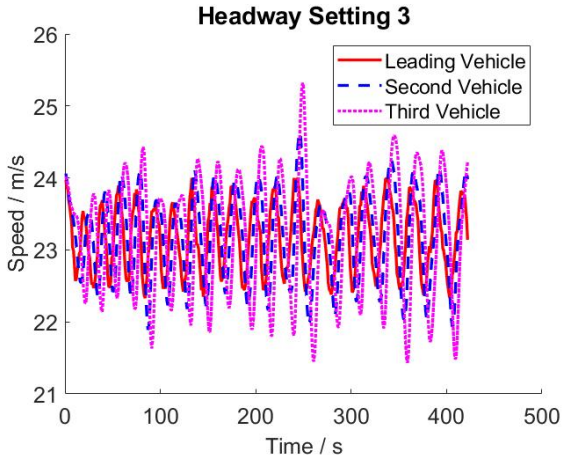

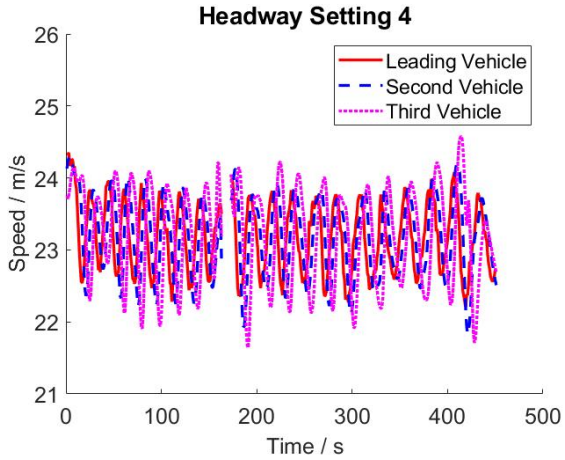

Outline

Field Experiments

Theoretical Analysis

Implication to Macroscopic Traffic

Preliminary results of Task 2: AV tradeoffs

❖ **ACC following distance decomposition**

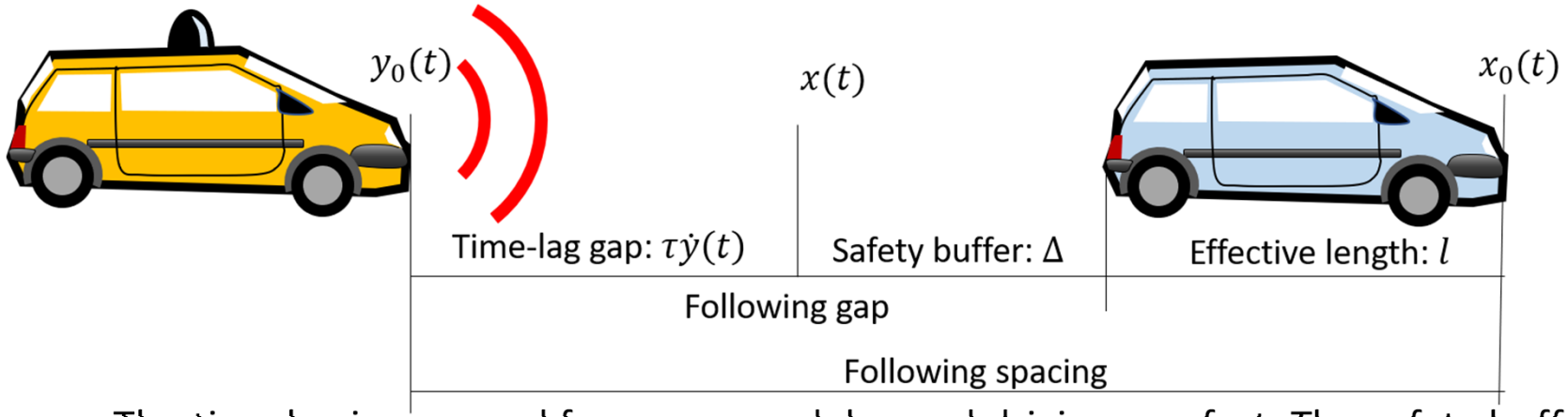

The time lag is reserved for response delay and driving comfort. The safety buffer is reserved to absorb the overshoot caused by the following vehicle due to the uncertainty of preceding vehicle's movements.

$$\ddot{y_0}(t) = \kappa\left(x_0(t) - l - \Delta - y_0(t) - \tau\dot{y_0}(t)\right)$$

where $x(t)$ and $y(t)$ are the locations (of the front bumpers) of the preceding and following vehicles at time t, $k > 0$ is the control sensitivity factors, $\Delta \geq 0$ is the safety buffer, $\tau \geq 0$ is the time lag, $l > 0$ is the preceding vehicle's length.

Safety Buffer Model

$$\text{RSB} : \Delta := \max_{T \in \mathbb{R}^+ := [0,\infty)} \Delta(T) := \max_{x_0, y_0, v_0, w_0, a_0} y_0(T) - (x_0(T) - l - \Delta)$$

Initial Conditions

$$\begin{aligned} \underline{v} \leq v_0(0) = w_0(0) \leq V, \\ x_0(0) - y_0(0) = l + \Delta + \tau w_0(0), \end{aligned}$$

Dynamics

$$\begin{aligned} \dot{x_0}(t) = v_0(t), \forall t \in \mathbb{R}^+, \\ \dot{v_0}(t) = a(t), \forall t \in \mathbb{R}^+, \\ \dot{w_0}(t) = \kappa \left(x_0(t) - l - \Delta - y_0(t) - \tau w_0(t) \right), \forall t \in \mathbb{R}^+, \end{aligned}$$

Kinetic Limits

$$\begin{aligned} \underline{v} \leq v_0(t) \leq V, \forall t \in \mathbb{R}^+, \\ -\bar{a} \leq a(t) \leq \bar{a}, \forall t \in \mathbb{R}^+. \end{aligned}$$

Analytical Solution

$$\Delta = \begin{cases} -\tau \underline{v}, & \text{if } \kappa\tau^2 \geq 4; \\ \left(1 - e^{-\frac{2\pi\theta}{\phi}}\right)^{-1} \left[A_1\left((2\alpha+\beta)/\phi - \bar{\delta}\right) E + A_2\left((2\alpha+\beta)/\phi - \bar{\delta}\right) \dot{E}\right] - \tau \underline{v}, & \text{if } \kappa\tau^2 < 4, \end{cases}$$

Where:

$$\alpha := \arcsin \frac{\theta}{\sqrt{\kappa}},$$

$$\beta := \begin{cases} \arctan \frac{e^{\theta\bar{\delta}} \sin(\phi\bar{\delta})}{e^{\theta\bar{\delta}} \cos(\phi\bar{\delta}) - 1}; & \text{if } e^{\theta\bar{\delta}} \cos(\phi\bar{\delta}) \text{-} 1 \geq 0, \\ \arctan \frac{e^{\theta\bar{\delta}} \sin(\phi\bar{\delta})}{e^{\theta\bar{\delta}} \cos(\phi\bar{\delta}) - 1} + \pi, & \text{if} e^{\theta\bar{\delta}} \cos(\phi\bar{\delta}) - 1 < 0, \end{cases}$$

$$\bar{\delta} := \min\{\bar{v}/\bar{a}, \pi/\phi\},$$

$$\theta := \frac{\kappa\tau}{2}, \phi := \frac{\sqrt{4\kappa - \kappa^2\tau^2}}{2},$$

$$\begin{aligned} E = {} & B_3\left(\bar{\delta}\right) + \sum_{l_3 \in \{1,2\}} A_{l_3}\left(\bar{\delta}\right) \otimes_{l_3} B_2\left(\pi/\phi - \bar{\delta}\right) \\ & + \sum_{l_3, l_2 \in \{1,2\}} A_{l_3}\left(\bar{\delta}\right) \otimes_{l_3} A_{l_2}\left(\pi/\phi - \bar{\delta}\right) \otimes_{l_2} B_1\left(\bar{\delta}\right) \\ & + \sum_{l_3, l_2, l_1 \in \{1,2\}} A_{l_3}\left(\bar{\delta}\right) \otimes_{l_3} A_{l_2}\left(\pi/\phi - \bar{\delta}\right) \otimes_{l_2} A_{l_1 1}\left(\bar{\delta}\right) \otimes_{l_1} B_4\left(\pi/\phi - \bar{\delta}\right), \end{aligned}$$

$$\begin{aligned} \dot{E} = {} & \dot{B}_3\left(\bar{\delta}\right) + \sum_{l_3 \in \{1,2\}} \dot{A}_{l_3}\left(\bar{\delta}\right) \otimes_{l_3} B_2\left(\pi/\phi - \bar{\delta}\right) \\ & + \sum_{l_3, l_2 \in \{1,2\}} \dot{A}_{l_3}\left(\bar{\delta}\right) \otimes_{l_3} A_{l_2}\left(\pi/\phi - \bar{\delta}\right) \otimes_{l_2} B_1\left(\bar{\delta}\right) \\ & \sum_{l_3, l_2, l_1 \in \{1,2\}} \dot{A}_{l_3}\left(\bar{\delta}\right) \otimes_{l_3} A_{l_2}\left(\pi/\phi - \bar{\delta}\right) \otimes_{l_2} A_{l_1}\left(\bar{\delta}\right) \otimes_{l_1} B_4\left(\pi/\phi - \bar{\delta}\right), \end{aligned}$$

$$A_1(t) = \frac{\sqrt{k}}{\phi} e^{-\theta t} \cos(\phi t - \alpha),$$

$$A_2(t) = \frac{1}{\phi} e^{-\theta t} \sin(\phi t),$$

$$B_j(t) := B_b(t) b_j + B_c(t) c_j,$$

$$B_b(t) = -2\tau t - \frac{2}{\kappa}\left(\kappa\tau^2 - 1\right)\left(e^{-\theta t}\cos(\phi t) - 1\right) - \frac{1}{\phi}\tau\left(\kappa\tau^2 - 3\right) e^{-\theta t}\sin(\phi t),$$

$$B_c(t) = -\tau + \tau\frac{\sqrt{k}}{\phi} e^{-\theta t}\cos(\phi t - \alpha),$$

$$\dot{B}_j(t) := \dot{B}_b(t) b_j + \dot{B}_c(t) c_j,$$

$$\dot{B}_b(t) = 2\tau\left(e^{-\theta t}\cos(\phi t) - 1\right) - \frac{1}{\phi}\left(2 - 2\tau\theta\right) e^{-\theta t}\sin(\phi t),$$

$$\dot{B}_c(t) = -\frac{\tau\kappa}{\phi} e^{-\theta t}\sin(\phi t),$$

$$b_1 = 0.5\bar{a}, b_2 = 0, b_3 = -0.5\bar{a}, b_4 = 0,$$

$$c_1 = 0, c_2 = \bar{a}\bar{\delta}, c_3 = \bar{a}\bar{\delta}, c_4 = 0,$$

$$A \otimes_1 B := AB, A \otimes_2 B := A\dot{B}.$$

Special Solutions

$$\Delta = \begin{cases} -\tau \underline{v}, & \text{if } \kappa\tau^2 \geq 4; \\ \bar{a}\left(\dfrac{1}{\kappa e^{\frac{2\arcsin\frac{\sqrt{\kappa}\tau}{2}}{\sqrt{4\kappa^{-1}\tau^{-2}-1}}}} + \dfrac{2}{\kappa e^{\frac{2\arcsin\frac{\sqrt{\kappa}\tau}{2}}{\sqrt{4\kappa^{-1}\tau^{-2}-1}}}\left(e^{\frac{\pi}{\sqrt{4\kappa^{-1}\tau^{-2}-1}}}-1\right)} \right) - \tau \underline{v}, & \text{if } \kappa\tau^2 < 4, \end{cases} \text{when } \bar{v}/\bar{a} \geq \pi/\phi. \qquad (24)$$

Proposition 3. *When $\bar{v}/\bar{a} \geq \pi/\phi$, Δ decreases with both κ and τ, and the decreasing trend is convex with $\Delta \to \infty$ as $\kappa \to 0$ or $\tau \to 0$ and $\Delta \to -\tau\underline{v}$ as $\kappa \to \infty$ or $\tau \to \infty$.*

Special Solutions

$$\Delta \to \begin{cases} -\tau \underline{v}, & \text{if } \kappa\tau^2 \geq 4; \\ \dfrac{\bar{v}}{\sqrt{k}e^{\frac{\arcsin\frac{\sqrt{\kappa}\tau}{2}}{\sqrt{4\kappa^{-1}\tau^{-2}-1}}}\left(e^{\frac{0.5\pi}{\sqrt{4\kappa^{-1}\tau^{-2}-1}}}-e^{-\frac{0.5\pi}{\sqrt{4\kappa^{-1}\tau^{-2}-1}}}\right)} - \tau\underline{v}, & \text{if } \kappa\tau^2 < 4, \text{ when } \bar{v}/\bar{a} \to 0. \end{cases}$$

Proposition 4. *When $\bar{v}/\bar{a} \to 0$, Δ decreases with both κ and τ, and the decreasing trend is convex with $\Delta \to \infty$ as $\kappa \to 0$ or $\tau \to 0$ and $\Delta \to -\tau\underline{v}$ as $\kappa \to \infty$ or $\tau \to \infty$.*

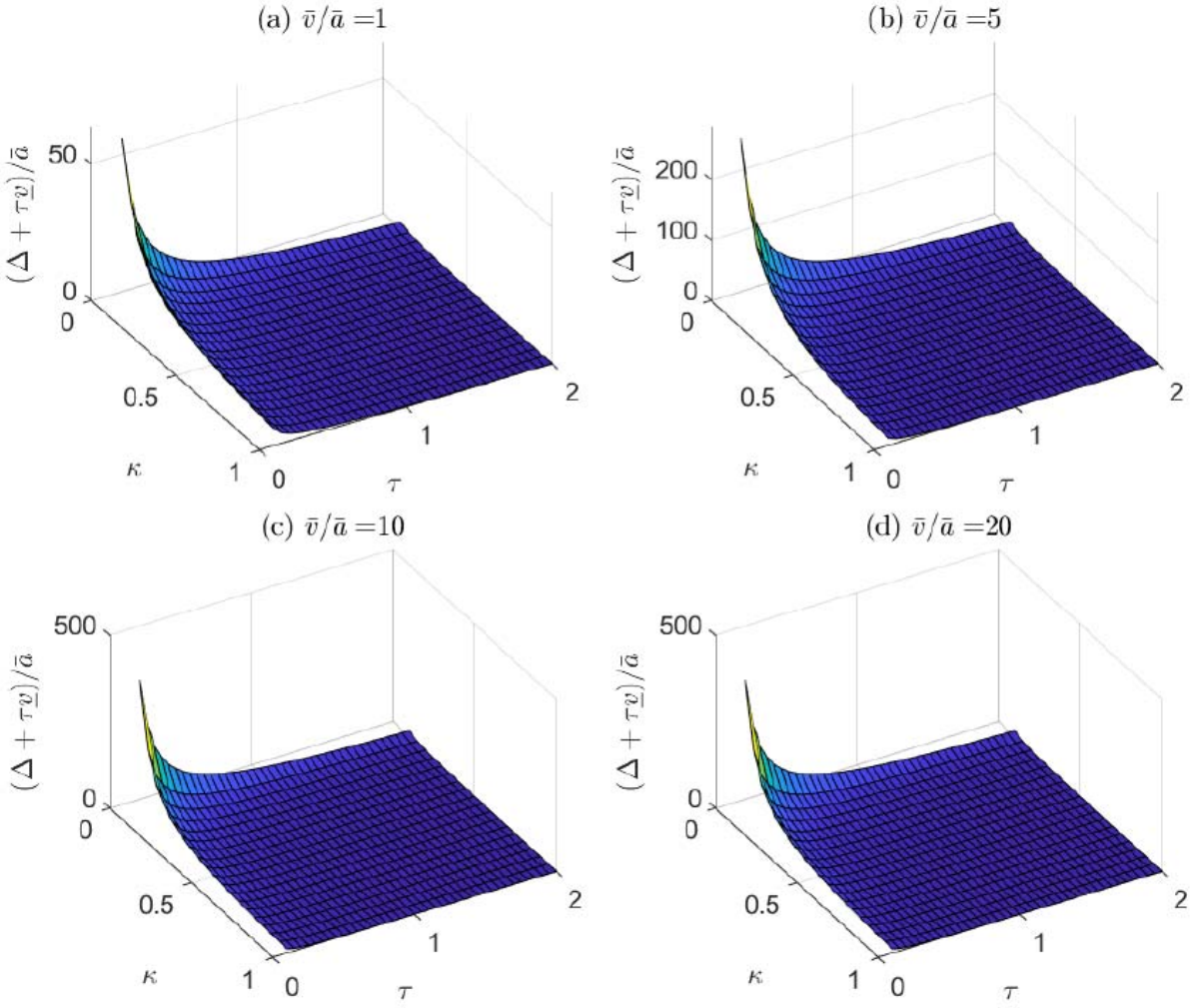
(a) $\bar{v}/\bar{a}$ =1
(b) $\bar{v}/\bar{a}$ =5
(c) $\bar{v}/\bar{a}$ =10
(d) $\bar{v}/\bar{a}$ =20
$(\Delta + \tau\underline{v})/\bar{a}$
κ
τ
0
0.5
1
2
50
100
200
500

Preliminary results of Task 2: AV tradeoffs

❖ **Parameter estimations**

	τ (s)	k	Δ (m)	R^2_{adj}
High Speed-Headway Setting 1	0.83	0.10	4.83	0.87
High Speed-Headway Setting 2	1.21	0.10	4.40	0.95
High Speed-Headway Setting 3	1.61	0.09	3.31	0.92
High Speed-Headway Setting 4	2.17	0.07	0.66	0.84
Low Speed-Headway Setting 1	0.79	0.12	7.28	0.92
Low Speed-Headway Setting 2	1.14	0.09	6.36	0.90
Low Speed-Headway Setting 3	1.52	0.08	5.92	0.83
Low Speed-Headway Setting 4	2.09	0.08	4.97	0.82

- The adjusted R^2 values for the model across all the settings are above 0.82, which indicates fairly good predictability of this model.

Experiment Results

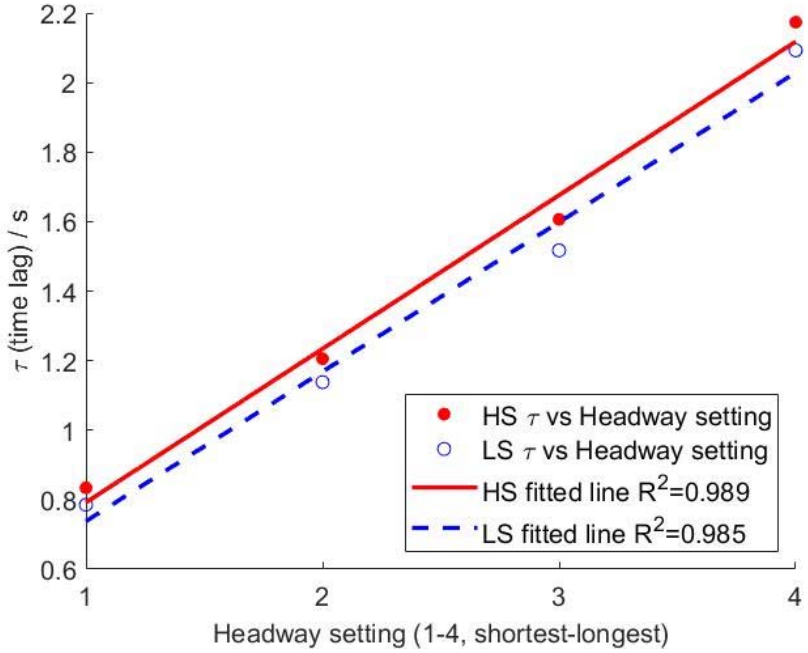

Following gap headway = time lag + (safety buffer/speed)

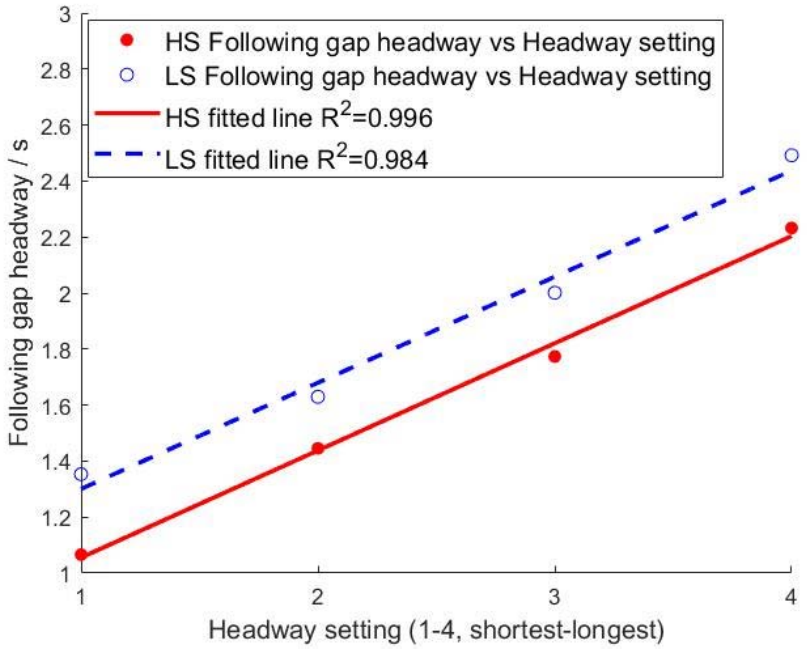

- The headway settings are highly correlated with the estimated time lags and following gap headway in linear relationships.

Experiment Results

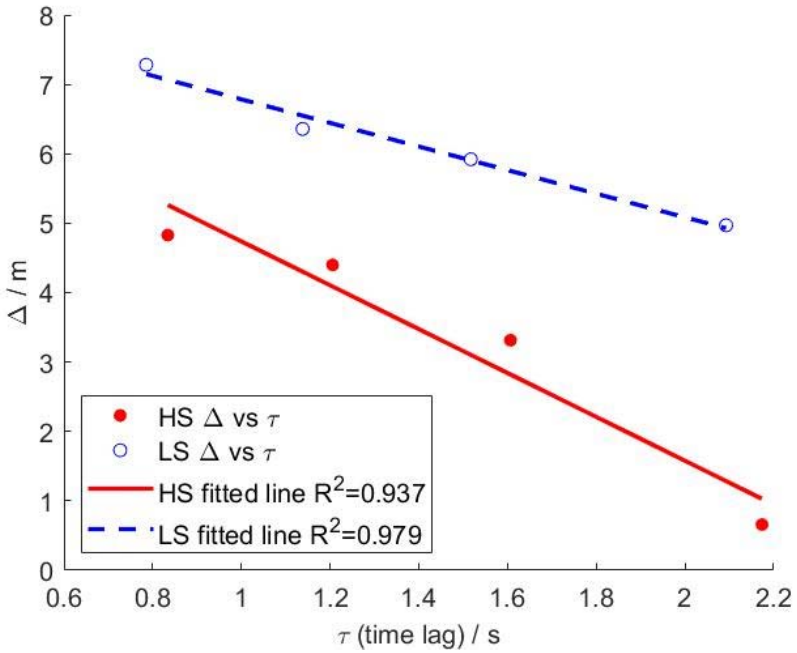

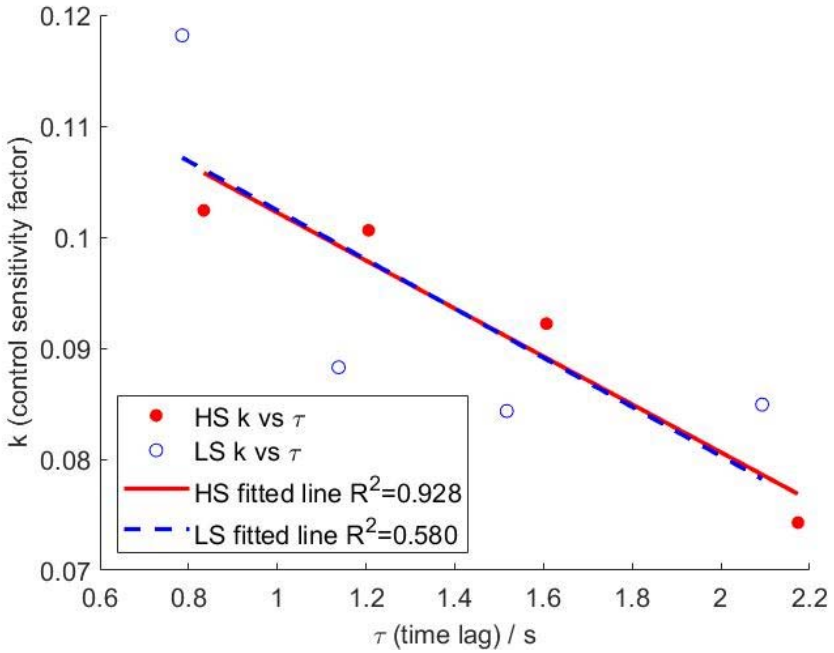

- A shorter time-lag gap (i.e., τ) demands a longer safety spacing buffer (i.e., Δ) to absorb a higher overshoot from the target trajectory in vehicle following control.
- The studied ACC system automatically adjust the vehicle control sensitivity to fit different driving environments.

Stability Analysis

- System frequency-domain transfer function

$$TF(\omega) := \frac{Y(j\omega)}{X(j\omega)} = \frac{\kappa}{-\omega^2 + \kappa + i\kappa\tau\omega}, \forall \omega \in \mathbb{R}^+$$

$$TF^* := \max_{\omega \in \mathbb{R}^+} |TF(\omega)| = \begin{cases} \sqrt{\frac{4}{4\kappa\tau^2 - \kappa^2\tau^4}} > 1, & \text{if } \kappa\tau^2 < 2; \\ 1 & \text{if } \kappa\tau^2 \geq 2, \end{cases}$$

$$\omega^* := \begin{cases} \sqrt{4\kappa - 2\kappa^2\tau^2}/2, & \text{if } \kappa\tau^2 < 2; \\ 0, & \text{if } \kappa\tau^2 \geq 2. \end{cases}$$

Preliminary results of Task 2: AV tradeoffs

❖ **Result analyses**

	$k\tau^2$	w^*	T^* (s)	Stability
High Speed-Headway Setting 1	0.07	0.31	19.99	Unstable
High Speed-Headway Setting 2	0.15	0.31	20.58	Unstable
High Speed-Headway Setting 3	0.24	0.29	22.04	Unstable
High Speed-Headway Setting 4	0.35	0.25	25.39	Unstable
Low Speed-Headway Setting 1	0.07	0.34	18.62	Unstable
Low Speed-Headway Setting 2	0.11	0.29	21.78	Unstable
Low Speed-Headway Setting 3	0.19	0.28	22.77	Unstable
Low Speed-Headway Setting 4	0.37	0.26	23.90	Unstable

- Results show that the studied AV following model is string unstable. A small speed variation of the preceding vehicle gets amplified while propagating across multiple following vehicles.
- We predict the cycle time of the perturbation (T*) caused by the speed variation.

Experiment Results

❖ Result analyses

	T=18	T=20	T=22	T=24	T=26
Headway 1	1.304	1.553*	1.505	1.515	1.478
Headway 2	1.378	1.460*	1.403	1.446	1.424
Headway 3	1.270	1.215	1.440*	1.253	1.352
Headway 4	1.142	1.199	1.201	1.148	1.208*

The predicted T^* for headways 1-4 respectively are 19.99 s, 20.58 s, 22.04 s, 25.39 s.

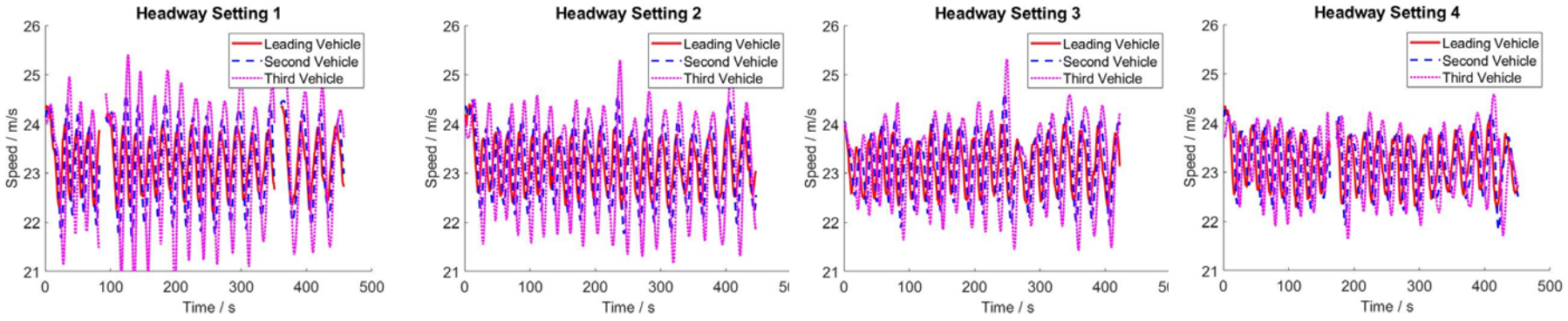

- As τ increases, the ACC control will be less unstable in terms of the oscillation amplifications and cycle periods.

Verification with Other Data

	Maker 1					Maker 2				
	τ (s)	k	Δ (m)	R^2_{adj}	$k\tau^2$	τ (s)	k	Δ (m)	R^2_{adj}	$k\tau^2$
Headway Setting Long	2.57	0.03	2.99	0.62	0.23	2.11	0.08	3.42	0.60	0.36
Headway Setting Short	1.13	0.04	7.41	0.59	0.05	1.05	0.06	8.59	0.68	0.07

- The values of Δ increase as τ decrease;
- The studied AV following designs still are string-unstable;
- As the values of τ (i.e., headway setting) increases, the control will be less unstable.

Gunter, G., Gloudemans, D., Stern, R.E., McQuade, S., Bhadani, R., Bunting, M., Monache, M.L.D., Lysecky, R., Seibold, B., Sprinkle, J., Piccoli, B., Work, D.B., 2019. Are commercially implemented adaptive cruise control systems string stable? 19122, 1–22.

Implication to Mobility

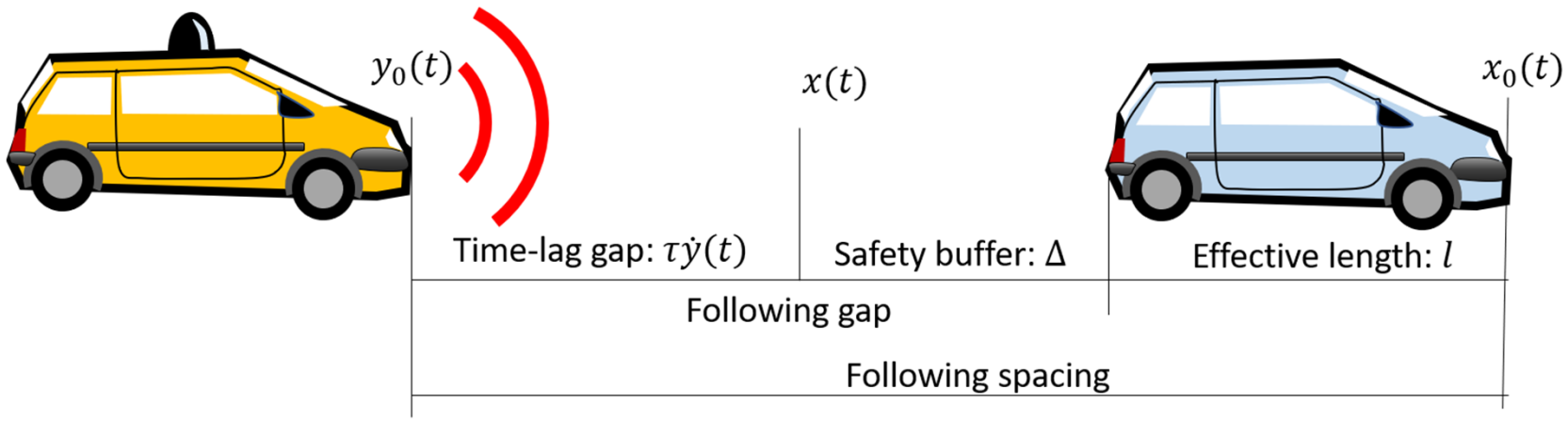

Gap headway

$$g = \frac{x(t) + \Delta - y_0(t)}{\bar{v}} = \frac{\Delta(\tau)}{\bar{v}} + \tau$$

Minimum Headway Design

- String-stable gap headway

$$\underline{g} = \frac{\Delta(\tau = \sqrt{k/2})}{\bar{v}} + \sqrt{k/2}$$

  A large value

- Varying time lag τ, minimizing following gap headway g

$$g^* := \min_{\tau} g := \frac{\Delta(\tau)}{\bar{v}} + \tau$$

Minimum Headway Design

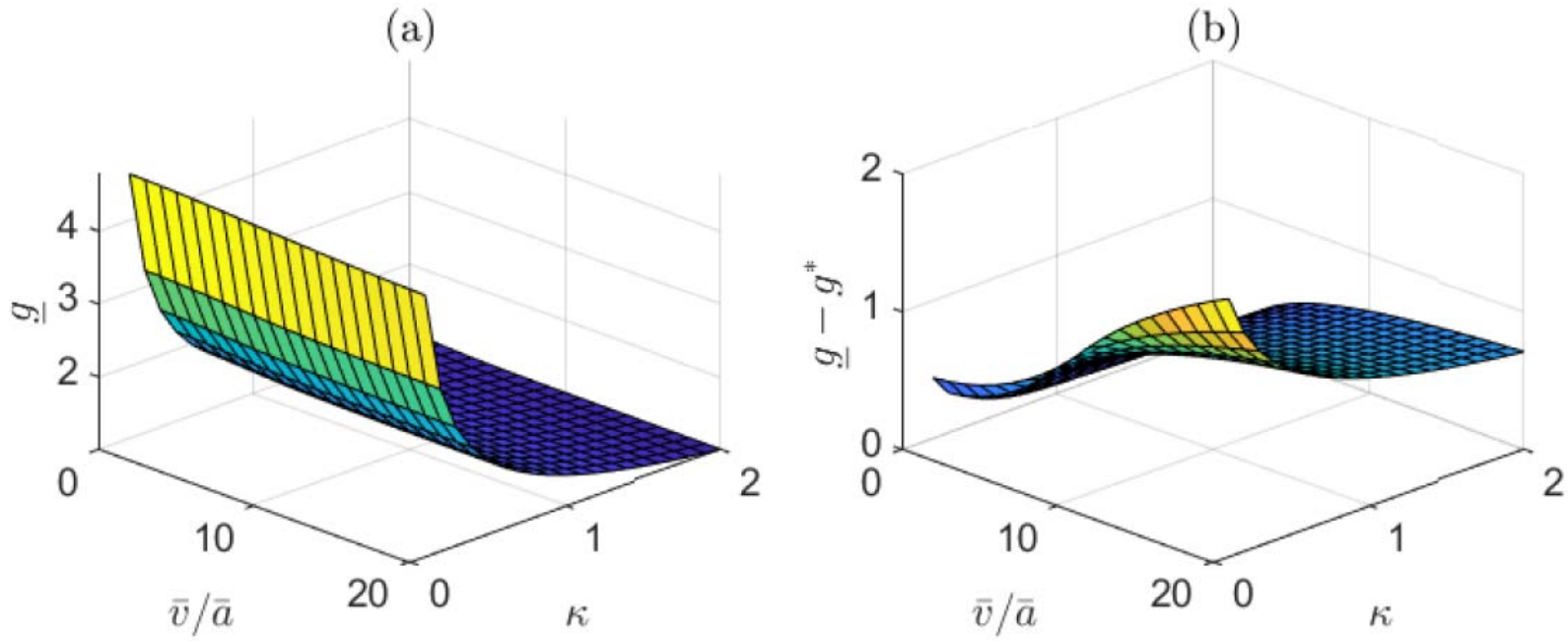

Implications to Commercial AV Makers

- Stability gap headway $\underline{g}$ is too long
- Compromise: a sweet spot between $\underline{g}$ and g^*
- AV makers do not care string stability
- The design gap headway is closer to g^*

Outline

Field Experiments

Theoretical Analysis

Implication to Macroscopic Traffic

AV FD

❖ Traffic flow characteristics calculation methods

- Macroscopic method

When a steam of trajectory data are available, we can study the traffic flow characteristics by the macroscopic method

$$k = \sum_{i=1}^{n} t_i/|A|, \qquad q = \sum_{i=1}^{n} x_i/|A|,$$

$$v = q/k = \sum_{i=1}^{n} x_i/t_i .$$

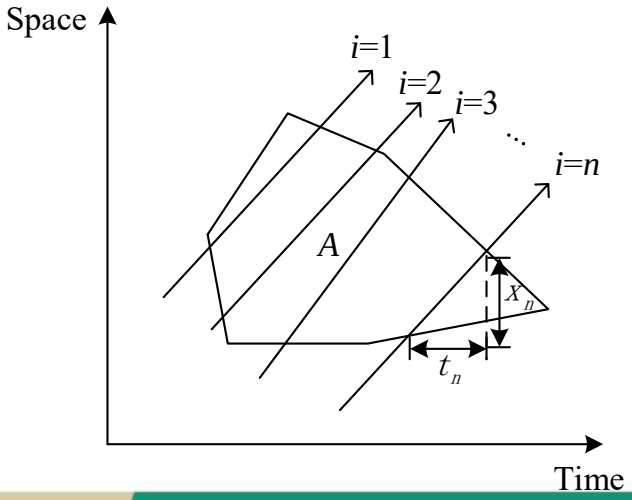

- Microscopic method

When the platoon is relatively short (e.g., only for a couple of vehicles), it would be difficult to apply the macroscopic method.

$$v = x/t, \quad k = t/|B|, \quad q = kv = x/|B|.$$

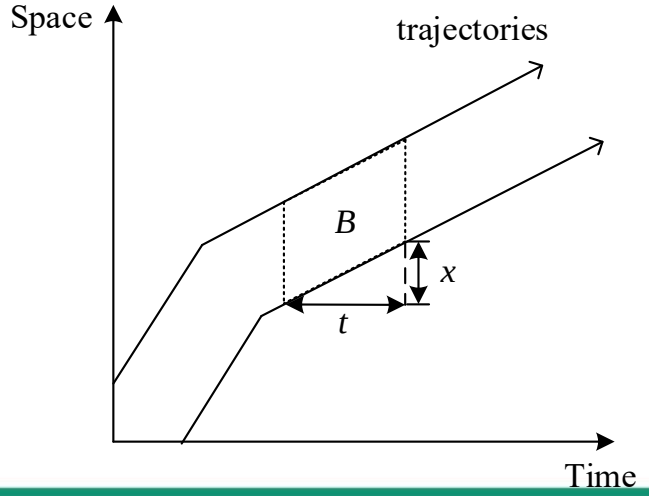

AV FD

❖ Datasets

- **Dataset 1**

  AV data collected by USF CATS team, including three-vehicle platoon trajectory data and car-following data

- **Dataset 2**

  AV data collected by another research team, including five-vehicle platoon trajectory data and car-following data

- **Dataset 3**

  HV traffic flow data extracted from videos shot by helicopters in a specified segment of Interstate 75 in Florida, US, by USF CATS team

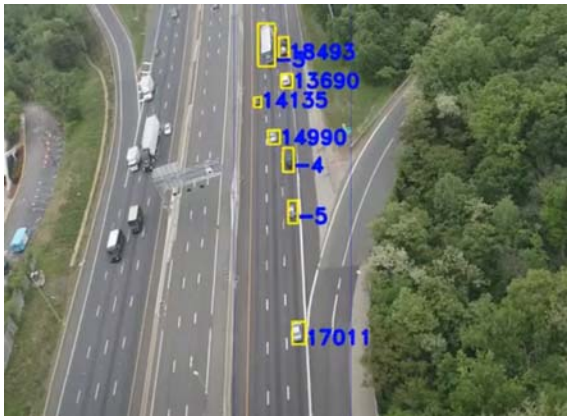

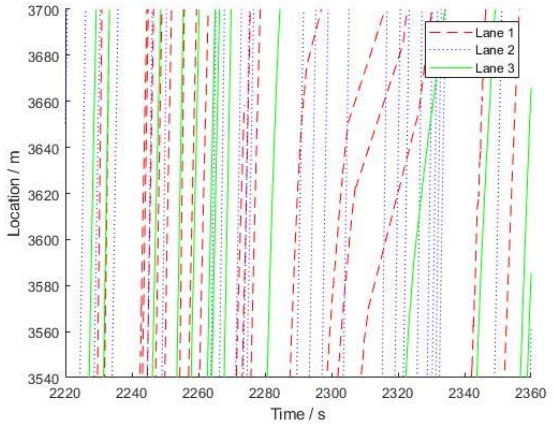

AV FD

❖ **Datasets 1: AV data collected by CATS team**

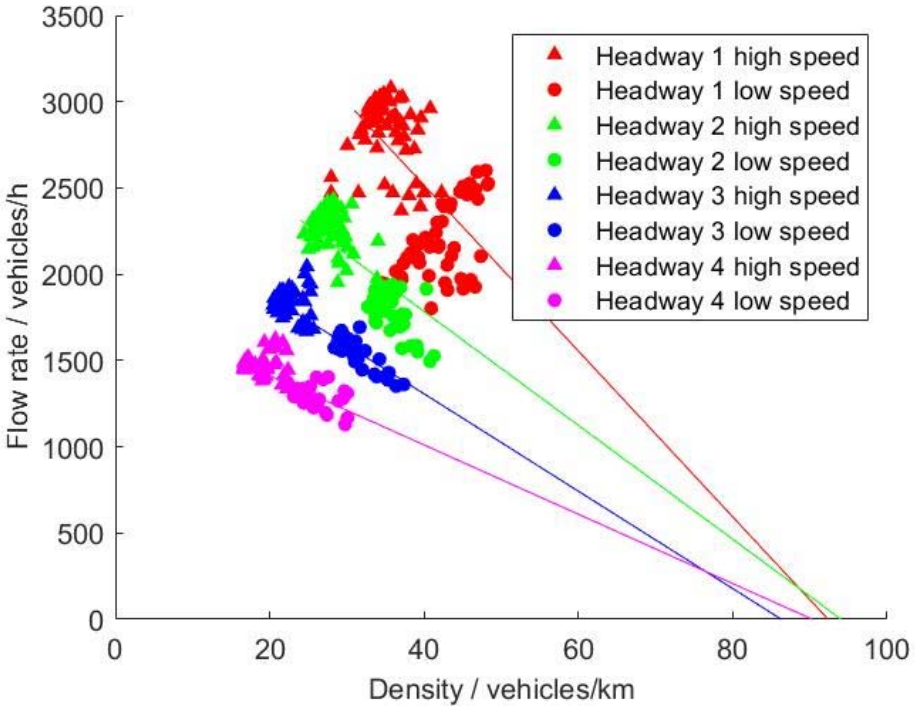

- As the density increases, the flow rate exhibits a decreasing trend.
- The longer the headway is, the lower the flow rate is, yet the slower the decreasing slope is.

- The road capacity (i.e., the maximum flow rate across all density) decreases as the AV headway setting increases.

AV FD

❖ **Datasets 2: AV data collected by Gunter et. al (2019)**

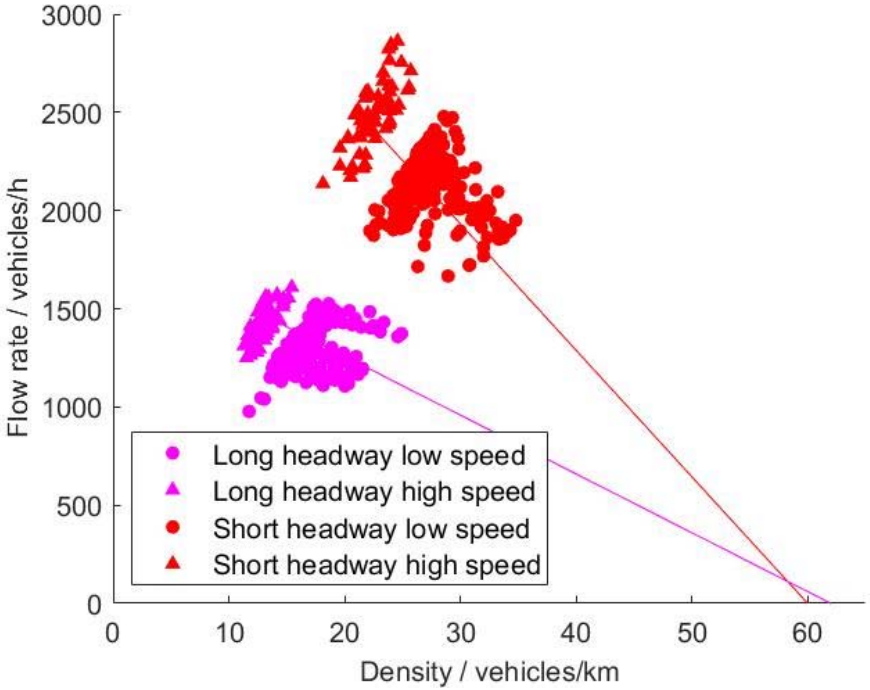

- As the density increases, the flow rate exhibits a decreasing trend.
- The jam density of Dataset 2 is smaller than Dataset 1.

Gunter, G., Gloudemans, D., Stern, R.E., McQuade, S., Bhadani, R., Bunting, M., Monache, M.L.D., Lysecky, R., Seibold, B., Sprinkle, J., Piccoli, B., Work, D.B., 2019. Are commercially implemented adaptive cruise control systems string stable? 19122, 1–22.

AV FD

❖ **Datasets 3: HV data collected by CATS team**

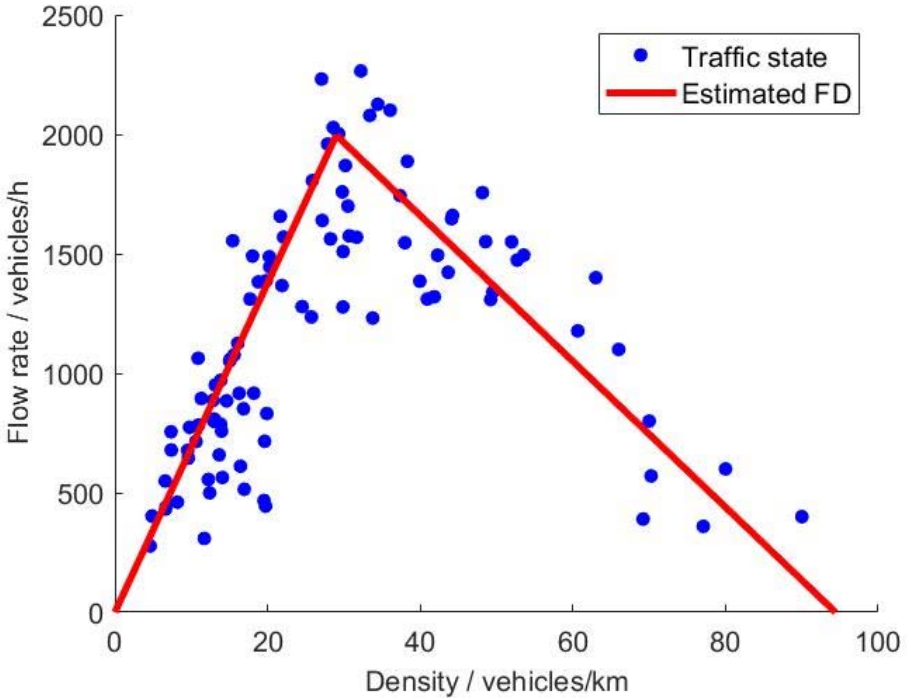

- Road capacity: 2000 vehicles/hour
- Jam density: 94.40 vehicles/km
- Adjusted R^2: 0.79

Zhao, D., Li, X., 2019. Real-World Trajectory Extraction from Aerial Videos - A Comprehensive and Effective Solution. 2019 IEEE Intell. Transp. Syst. Conf. ITSC 2019 2854–2859.

AV FD

❖ Estimation results

		Road capacity (vehicles/h)	Shock wave speed (km/h)	Jam density (vehicles/km)	Adjusted R^2
Dataset 1	**Headway 1**	2900	48.1	92.34	0.32
	Headway 2	2250	33.0	94.03	0.33
	Headway 3	1850	28.2	86.29	0.81
	Headway 4	1500	20.1	90.29	0.71
Dataset 2	**Headway short**	2550	64.4	62.00	0.10
	Headway long	1480	30.0	60.91	0.22
Dataset 3	**Human-driven**	2000	30.5	94.40	0.79

- The impacts of AVs on traffic flow are related to the enabled headway settings: a shorter headway setting improves the road capacity.
- The values of the minimum and maximum capacities across different AV vendors are consistent despite some minor discrepancies.
- The existing commercial AV following algorithms may be designed based on the traffic flow characteristics of human-driven vehicles.

AV FD

❖ **FD of mixed traffic**

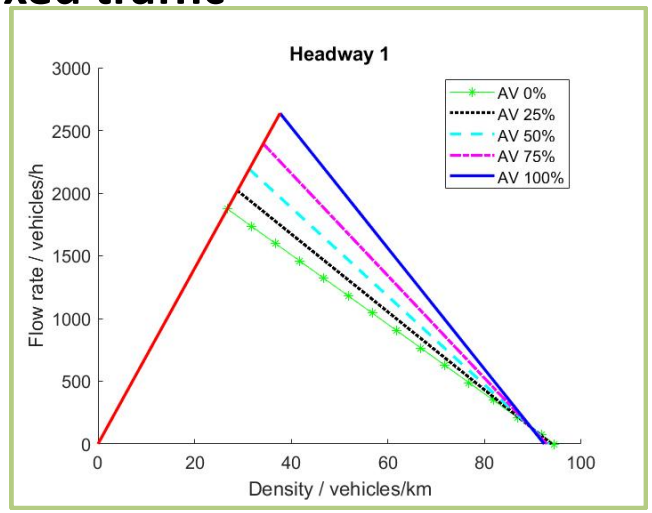

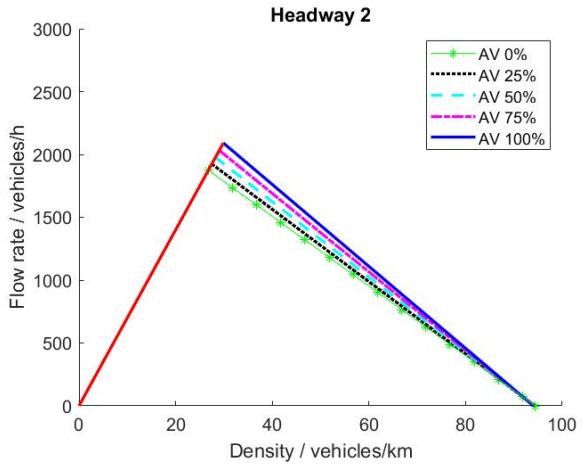

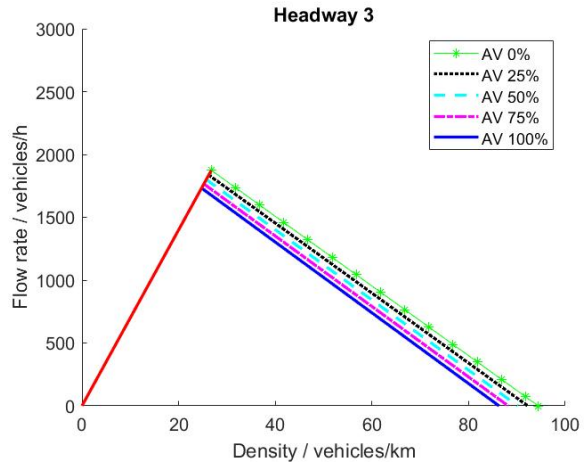

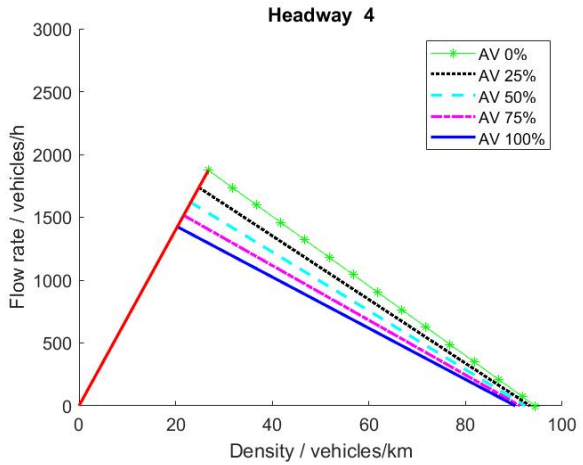

References

- Li, X. Trade-off between safety, mobility and stability in automated vehicle following control: An analytical method. Preprint. [http://dx.doi.org/10.13140/RG.2.2.28804.35204]
- Shi, X. and Li, X., 2020. Empirical Study on Car Following Characteristics of Commercial Automated Vehicles with Different Headway Settings. Preprint. [http://dx.doi.org/10.13140/RG.2.2.21464.32004/1]
- Shi, X. and Li, X., 2020. Constructing Fundamental Diagram for Traffic Flow with Automated Vehicles: Methodology and Demonstration. Preprint. [http://dx.doi.org/10.13140/RG.2.2.25353.67681]

Acknowledgement

- Xiaowei Shi (USF PhD Candidate)
- NSF CMMI CAREER # 1558887;
- NSF CPS #1932452;
- Special thanks to Zhaohui Liang, Peng Zhang, Handong Yao, Qianwen Li for helping collect the data, and to Chris Simpron from FDOT District 1 for providing valuable comments.

THANKS!
Q&A?

XIAOPENGLI@USF.EDU

UNIVERSITY of SOUTH FLORIDA